AIAA JOURNAL
Vol. 39, No. 7, July 2001

Numerical Analysis of Dusty Hypersonic Viscous Gas Flow over a Flat Plate

R. Padmapriya* and K. P. J. Reddy†
Indian Institute of Science, Bangalore 560 012, India

We present an analysis of dilute gas-particle flows at hypersonic Mach number in which the flow parameters are obtained by solving complete two-dimensional Navier–Stokes equations numerically for a flat-plate geometry. The conservation equations for both the gas and particle phases have been solved using finite volume upwind schemes. Time marching is carried out using the Euler-implicit scheme for the gas phase and the Euler-explicit scheme for the particle phase. Roe's flux-difference-splitting scheme is used for the gas phase, and the Steger–Warming flux-vector-splitting scheme is applied for the particle phase. The detailed flow structures of the gas and particle phases are given in three distinct regions: the large-slip region near the leading edge, the moderate-slip region, and the small-slip region far downstream. It is found that the presence of solid particles in the flow has an appreciable effect on the flowfield parameters. Also the presence of particles enhance the skin friction and heat transfer along the wall and decreases the boundary-layer thickness compared with the pure-gas case.

Nomenclature

C_d	=	drag coefficient of particle
c	=	local speed of sound
$\hat{c}$	=	speed of sound evaluated at Roe-averaged state
d_p^*	=	particle diameter
E	=	total energy of the gas phase
e	=	internal energy of the gas phase
F	=	column vector of flux in x direction
$\boldsymbol{F}$	=	flux vector
F_N	=	column vector of inviscid flux normal to an interface
F_{px}	=	drag force in the x direction
F_{py}	=	drag force in the y direction
G	=	column vector of flux in y direction
H	=	column vector of the interaction terms
M_∞	=	freestream Mach number
N_u	=	Nusselt number
Pr	=	Prandtl number
q_x, q_y	=	heat flux terms in x and y directions
Re_r	=	relative Reynolds number
Re_x	=	local Reynolds number
Re_∞	=	freestream Reynolds number
S	=	Sutherlands constant
T	=	gas temperature
u	=	gas velocity component in x direction
v	=	gas velocity component in y direction
β	=	particle loading ratio at freestream
Γ	=	particle material specific heat ratio
γ	=	ratio of specific heats
λ_∞^*	=	velocity equilibrium length
μ	=	gas viscosity
ρ	=	gas phase density
ρ_m	=	particle material density
τ_T	=	temperature relaxation time
τ_v	=	velocity relaxation time
τ_{xx}, τ_{xy}, τ_{yy}	=	shear stress terms

Subscripts

p	=	particle phase
w	=	quantities at the wall
∞	=	freestream quantities

Superscript

$*$	=	dimensional quantities

Received 21 October 1998; revision received 8 May 2000; accepted for publication 22 December 2000. Copyright © 2001 by the American Institute of Aeronautics and Astronautics, Inc. All rights reserved.

*Research Scholar, Department of Aerospace Engineering.
†Associate Professor, Department of Aerospace Engineering.

Introduction

MOST of the interplanetary explorations are dominated by the hypersonic flight corridors. The reentry aerodynamics of vehicles flying at hypersonic Mach numbers is an important aspect of most space missions. More often the composition of the atmosphere, which the vehicle has to encounter, consists of not only gas other than pure air but also dust particles of varying dimensions. Further, in the case of Martian entry probes using the ablative material for protection against the severe aerodynamic heating, which occurs at high flight velocities, the products of ablation particles are also present giving rise to a complex flows. Therefore it calls for a study of flows that is more realistic in nature, i.e., two-phase flows.

Dusty-gas flows have been studied by a number of authors[1–6] in the past because of their application in rocket nozzle flow, supersonic flight through dust clouds, and in the prediction of erosion damage caused by dust particles. A complete review of numerical models of dilute gas-particle flows has been presented by Crowe.[7] Soo,[8] Marble,[9] and Chiu[10] have studied incompressible laminar boundary-layer flow of dusty fluid over a semi-infinite flat plate. Because of the complexity of the problem, Soo has used integral method in his analysis. Chiu analyzed the dusty-gas flow using boundary-layer equations by neglecting the particle momentum equation in the normal direction. Singleton[11] extended Marble's analysis to the compressible case where the density of the gas phase as well as the particle phase may change. In the case of two-phase boundary-layer flows, Otterman[12] has shown that the standard boundary-layer approximations are valid for the fluid phase provided that the density of the particle phase is of the same order as that of the fluid. Wang and Glass[13] investigated the behavior of steady compressible laminar boundary-layer flows of a dilute dusty gas over a semi-infinite flat plate at supersonic Mach number using implicit finite difference method. Gas-particle flow in a solid rocket nozzle is analyzed by Hwang and Chang[14] numerically. Eulerian approach was used for the gas flow, whereas the Lagrangian approach was used to determine the velocity, position and temperature of particles. Chang et al.[15] developed a time-dependent numerical algorithm for the two-fluid model using Euler and thin-layer Navier–Stokes equations. The algorithm was applied to investigate Jet Propulsion Laboratory nozzle flow to show performance inefficiencies arising from the effect of particles.

Although the literature on this subject is very rich, most of the theoretical work done was based on the approximate forms of Navier–Stokes equations. Apart from this many of these analyses were restricted to a particular region in the flowfield such as the stagnation

point. These analyses, despite the approximations involved at various levels, have given good physical insight into the subject. Nevertheless, owing to the approximations made in these analyses, their results will have limited applications. Often, it is very difficult to say whether the solutions through these analyses are unique,[16] unless a less approximate analysis confirms it. Moreover, for cases where flow separation or a shock-shock or shock-boundary-layer interaction occurs, such an analysis cannot be made. Thus, the present paper aims at a more accurate study of gas-particle flows at hypersonic Mach number by solving complete two-dimensional Navier–Stokes (N–S) equations coupled with particle-phase equations numerically.

Governing Equations

In this analysis the gas-particle mixture is assumed as a dilute two-phase system where the volume fraction of the particles is neglected. Also, we have ignored the radiative heat transfer, chemical reactions, coagulations, phase change, and deposition in the system of equations presented here. The gas phase is a perfect gas, and the particle phase is treated as a continuum consisting of small solid particles of uniform size. The particles have a constant specific heat, and the internal temperature of the particles is uniform. The particles have no individual random motion, mutual collisions, and other interactions among them. Only the process of drag and heat transfer couple the particles with the gas. The drag coefficient and the Nusselt number for a single sphere in a viscous flow are assumed valid for the particle cloud.

With the preceding assumptions the nondimensional N–S equations governing the dusty-gas flow can be written in the conservative form[17] as

$$\frac{\partial U}{\partial t}+\frac{\partial F_I}{\partial x}+\frac{\partial G_I}{\partial y}-\frac{\partial F_V}{\partial x}-\frac{\partial G_V}{\partial y}=H \tag{1}$$

$$\frac{\partial U_p}{\partial t}+\frac{\partial F_P}{\partial x}+\frac{\partial G_P}{\partial y}=H_p \tag{2}$$

where

$$U=\begin{bmatrix}\rho\\ \rho u\\ \rho v\\ \rho E\end{bmatrix},\qquad F_I=\begin{bmatrix}\rho u\\ \rho u^2+p\\ \rho uv\\ u(\rho E+p)\end{bmatrix}$$

$$G_I=\begin{bmatrix}\rho v\\ \rho uv\\ \rho v^2+p\\ v(\rho E+p)\end{bmatrix},\qquad F_V=\begin{bmatrix}0\\ \tau_{xx}\\ \tau_{xy}\\ u\tau_{xx}+v\tau_{xy}-\dot q_x\end{bmatrix}$$

$$G_V=\begin{bmatrix}0\\ \tau_{xy}\\ \tau_{yy}\\ u\tau_{xy}+v\tau_{yy}-\dot q_y\end{bmatrix},\qquad H=\begin{bmatrix}0\\ F_{px}\\ F_{py}\\ u_pF_{px}+v_pF_{py}+Q_p\end{bmatrix}$$

for the gas phase,

$$U_p=\begin{bmatrix}\rho_p\\ \rho_p u_p\\ \rho_p v_p\\ \rho_p E_p\end{bmatrix},\qquad F_P=\begin{bmatrix}\rho_p u_p\\ \rho_p u_p^2\\ \rho_p u_p v_p\\ \rho_p u_p E_p\end{bmatrix}$$

$$G_p=\begin{bmatrix}\rho_p v_p\\ \rho_p u_p v_p\\ \rho_p v^2\\ \rho_p v_p E_p\end{bmatrix},\qquad H_p=\begin{bmatrix}0\\ -F_{px}\\ -F_{py}\\ -u_pF_{px}-v_pF_{py}-Q_p\end{bmatrix}$$

for the particle phase, and

$$\tau_{xx}=\frac{1}{Re_\infty}[\lambda(u_x+v_y)+2\mu u_x],\qquad \tau_{xy}=\frac{1}{Re_\infty}[\mu(u_y+v_x)]$$

$$\tau_{yy}=\frac{1}{Re_\infty}[\lambda(u_x+v_y)+2\mu v_y],\qquad \dot q_x=\frac{-\mu}{(\gamma-1)M_\infty^2Re_\infty Pr}\frac{\partial T}{\partial x}$$

$$\dot q_y=\frac{-\mu}{(\gamma-1)M_\infty^2Re_\infty Pr}\frac{\partial T}{\partial y},\qquad \rho E=\frac{p}{\gamma-1}+\frac{\rho}{2}(u^2+v^2)$$

$$\rho_pE_p=\frac{\Gamma\rho_pT_p}{(\gamma-1)M_\infty^2}+\frac{\rho_p}{2}\left(u_p^2+v_p^2\right)$$

Here, the flow parameters are nondimensionalized with respect to the freestream conditions, and the length parameters are nondimensionalized with respect to the particle velocity equilibrium length, defined as $\lambda_\infty^*=\rho_m^*d_m^{*2}u_\infty^*/18\mu_\infty^*$. The two sets of Eqs. (1) and (2) are coupled through the momentum interchange force and the heat transfer. If the drag coefficient for the particles is assumed to be of the Stokes form,[18] $C_d=24/Re_r$, then the drag forces in the nondimensional form are given by

$$F_{px}=\mu\rho_p(u_p-u)/\tau_v \tag{3a}$$

$$F_{py}=\mu\rho_p(v_p-v)/\tau_v \tag{3b}$$

where

$$\tau_v=\frac{\rho_m^*d_m^{*2}U_\infty^*}{18\mu_\infty^*\lambda_\infty^*}$$

The heat-transfer coefficient between the gas and particles is given by

$$Q_p=\frac{\Gamma\mu\rho_p}{(\gamma-1)M_\infty^2\tau_T}N_u(T_p-T) \tag{4}$$

where the Nusselt-number correlation used is of the form[19] $N_u=2+0.6Pr^{(1/3)}Re_r^{(1/2)}$ and

$$\tau_T=\frac{\Gamma\,Pr\,\rho_m^*d_m^{*2}U_\infty^*}{6\mu_\infty^*\lambda_\infty^*}$$

The nondimensional thermal and caloric equation of state for the gas phase can be expressed as

$$p=\rho\bar RT \tag{5}$$

where $\bar R=(1/\gamma M_\infty^2)$ is the specific gas constant.

In the present analysis it is assumed that the viscosity-temperature relation for gas phase is based on Sutherlands law given by

$$\mu=T^{\frac{3}{2}}[(1+S)/(T+S)] \tag{6}$$

The problem contains nine unknowns u, u_p, v, v_p, p, ρ, ρ_p, T, and T_p governed by the preceding set of eight equations along with the equation of state for the gas phase, which will close the problem.

Numerical Algorithm and Validation

Even though the system of equations is written in the elaborate form, the sensitive problem of the choice of the numerical method is still to be addressed. As mentioned before, the finite volume method is applied to solve the gas-particle flow problems, which allows accurate treatment of the discontinuity between the one-phase flow and the two-phase flow because of the computation of fluxes at the cell boundaries via the resolution of the Riemann problem. The numerical treatments for the gas and particle phases are given in the following descriptions.

Gas Phase

The inviscid terms of the gas phase are treated using Roe's flux difference scheme.[20] In this scheme the interface at which the fluxes are to be evaluated is considered as a discontinuity with a left state U_l^- and a right state U_l^+. The details of the derivation of fluxes are

not presented here for the sake of brevity. The final form of the flux formulas is given by

$$(F_N)_l = \frac{1}{2}\left[F\left(U_l^-\right) + F\left(U_l^+\right)\right] - \left\{\sum_{k=1}^{4}\left|\hat{a}^{(k)}\right|\Delta V^{(k)} R^{(k)}\right\}_i \quad (7)$$

where $\hat{a}^{(1)} = \hat{u}_\perp - \hat{c}$, $\hat{a}^{(2)} = \hat{u}_\perp$, $\hat{a}^{(3)} = \hat{u}_\perp$, and $\hat{a}^{(4)} = \hat{u}_\perp + \hat{c}$ are the eigenvalues of the Roe's-averaged matrix. The right eigenvectors corresponding to the eigenvalues of the Roe's-averaged matrix are given by

$$\hat{R} = \begin{bmatrix} 1 & 0 & 1 & 1 \\ \hat{u} - \hat{c}\dfrac{\Delta y}{\Delta s} & \hat{c}\dfrac{\Delta x}{\Delta s} & \hat{u} & \hat{u} + \hat{c}\dfrac{\Delta y}{\Delta s} \\ \hat{v} + \hat{c}\dfrac{\Delta x}{\Delta s} & \hat{c}\dfrac{\Delta y}{\Delta s} & \hat{v} & \hat{v} - \hat{c}\dfrac{\Delta x}{\Delta s} \\ \hat{H} - \hat{c}u_\perp & \hat{u}_\parallel \hat{c} & \dfrac{\hat{u}^2 + \hat{v}^2}{2} & \hat{H} + \hat{c}u_\perp \end{bmatrix}$$

The characteristic variables are given as

$$\Delta V = \begin{bmatrix} (1/2\hat{c}^2)[\Delta(p) - \hat{\rho}\hat{c}\Delta(u_\perp)] \\ (\hat{\rho}/\hat{c})\Delta(u_\parallel) \\ [\Delta(\rho) - \Delta(p)/\hat{c}^2] \\ (1/2\hat{c}^2)[\Delta(p) + \hat{\rho}\hat{c}\Delta(u_\perp)] \end{bmatrix}$$

where $\Delta(\,) = (\,)^+ - (\,)^-$.

The symbol $\hat{}$ represents the averaged quantity and is defined as in Ref. 20. Viscous terms are treated using auxiliary cell approach.[21] The temporal descritization for the gas phase is carried out in Euler-implicit form. Line-Jacobi relaxation algorithm has been applied to the resulting set of equations.

Particle Phase

The Steger and Warming flux-vector-splitting technique[22] is used to determine the inviscid fluxes of the particle phase as there is only one eigenvalue in the convective flux. In this technique the flux vector is split into positive part $U_{\rm pl}$, and negative part $U_{\rm pr}$ by making use of similarity transformations and the homogeneity property of the Euler equations. The flux at the cell interface is determined using the relationship

$$(F_{p_N})_l = \left[F_p\left(U_p^+\right)_l + F_p\left(U_p^-\right)_r\right] = F_{p_N}^+ + F_{p_N}^- \quad (8)$$

where

$$F_{p_N}^{\pm} = u_{p\perp}^{\pm}\begin{bmatrix} \rho_p \\ \rho_p u_p \\ \rho_p v_p \\ \rho_p E_p \end{bmatrix}$$

$$u_{p\perp}^{\pm} = \frac{u_{p\perp} \pm |u_{p\perp}|}{2}, \qquad u_{p\perp} = u_p\frac{\Delta y}{\Delta s} - v_p\frac{\Delta x}{\Delta s}$$

in which $u_{p\perp}$ is the corresponding eigenvalue for the particle phase equations.

Thus, the numerical procedure for solving the particle-phase equations is described, and what remains is to implement the coupling between the two systems (gas and particles). The homogenous solutions of both systems being known, the solutions to the nonhomogenous system are obtained by integrating in time over the interaction terms. The temporal discretization for the particle phase is carried out in Euler-explicit form.

Boundary Conditions

The treatment of boundary conditions for dusty-gas flow is more subtle than in pure gasdynamics; in fact, it is, currently, still an open question. The boundary conditions for the gas phase are well known and do not pose any particular difficulties, as at each point with the flowfield and also on the boundaries an exact Riemann problem is solved. However, there is some experimental evidence that the particles experience some slip at the wall. Because the particle phase can resemble a rarefied gas, a boundary condition borrowed from rarefied-gas dynamics is utilized here. In reality the tangential velocity of the particle phase at the wall is controlled by many physical effects such as sliding friction, the nature of particle/surface collision, etc. It is not possible to model such effects with precision at present. Hence the physics of the present problem suggest the following boundary conditions for a flat plate.

At the wall of the flat plate:

$$u(x,0) = 0, \qquad v(x,0) = 0, \qquad T(x,0) = T_w$$

$$v_p(x,0) = 0, \qquad u_p(x,0) = 1 - \mu_w x$$

The tangential velocity distribution considered here for particle phase is taken from Ref. 13.

At the outer edge of the boundary layer:

$$u(x,\infty) = 1, \qquad T(x,\infty) = 1, \qquad u_p(x,\infty) = 1$$

$$T_p(x,\infty) = 1, \qquad \rho_p(x,\infty) = \beta$$

where β is the mass loading ratio of the particles. For the flat-plate problem it is assumed that the particle phase is in equilibrium with the gas phase in the external freestream, because there is no pressure gradient.

Results and Discussion

The N-S code is validated against the boundary-layer theory results by regenerating the dusty gas flowfield profiles. The finite difference solutions obtained from Ref. 13 are in the three flow regions known as the quasi-frozen flow region near the leading edge, the nonequilibrium flow region, and the quasi-equilibrium flow region far downstream, as shown in Fig. 1. The velocity and temperature flow profiles in these regions are compared with the present work for the same conditions as given in Ref. 13. The flat-plate wall temperature T_w is fixed at 0.5, and the results are compared for $M_\infty = 1.5$, $Re_\infty = 10^4$, and for particle size of 10 μm with the mass loading ratio $\beta = 1$. The solutions from the present analysis are found to be in good agreement with the boundary-layer solutions. The velocity and temperature profiles for the two phases in the boundary layer at $x = 0.109$ and 2.09 are plotted in Figs. 2a–3b, which show that there is a very large slip between the particle and gas phases in the near-leading-edge region and hence the flow is quasi-frozen. The results in the nonequilibrium region indicate that the slip between the particles and the gas diminishes gradually as x increases. However, in this transition region the particles still have moderate slip against the gas, and then the two-phase flow is characterized by nonequilibrium. Finally, the flow profiles in the small slip indicate that the quasi-equilibrium state between the particle and the gas has already been reached. The curves presented in these figures indicate an excellent agreement between the present solutions and those predicted using boundary-layer theory.

A grid-refinement study was made to determine the accuracy of the N-S code along the lines of Blottner.[23] The details of the grid-refinement study are given in Table 1. Here the grid types G1–G4

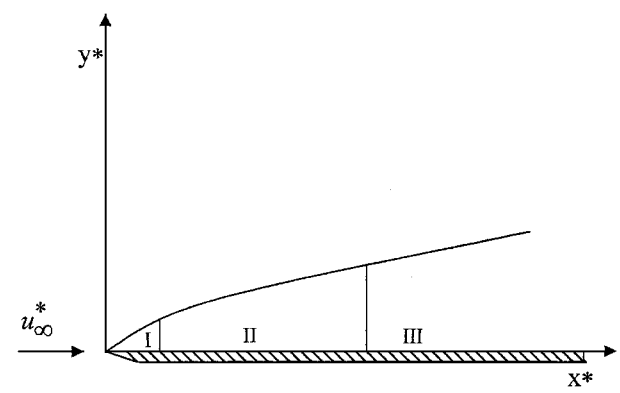

Fig. 1 Schematic representation of three distinct regions of dusty-gas flow over a flat plate: large slip region I, moderate slip region II, and small slip region III.

Table 1 Grid refinement in y direction; i max = 32, M_∞ = 6, and $Re_\infty = 10^6$

Grid type	j max	x 0.0000	0.2500	1.0000	1.50000	Error in
G1	22	−5.066	−0.0487	0.0033	0.0098	P_w
G2	44	0.0355	−0.0162	−0.1913	−0.1951	
G3	88	0.1865	0.0065	0.0000	0.0000	
G4	176	0.1565	−0.0162	−0.0032	0.0000	
G1	22	−8.2373	−3.0388	−0.0986	−0.2152	C_f
G2	44	−5.8098	−2.2916	−0.3331	−0.2985	
G3	88	−3.9819	−1.5945	−0.1940	−0.1568	
G4	176	−2.5280	−0.8914	−0.0875	−0.3078	
G1	22	−18.0451	−9.1133	−4.4856	−3.4867	q_w
G2	44	−13.1095	−5.7008	−2.4630	−1.8991	
G3	88	−8.9546	−3.4926	−1.2718	−0.9599	
G4	176	−5.7529	−1.9288	−0.6643	−0.7631	

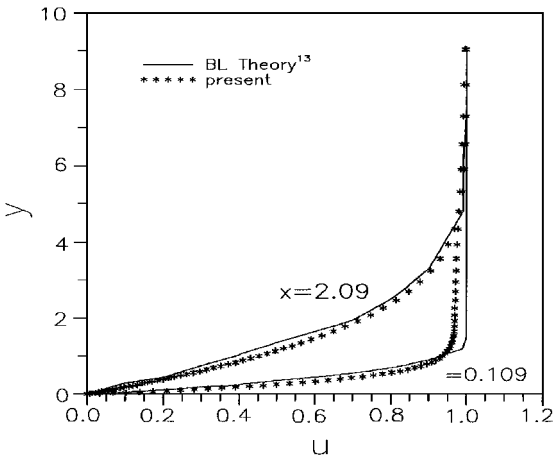

a)

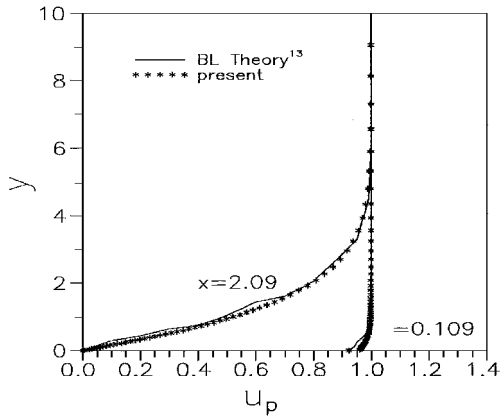

b)

Fig. 2 Comparison of a) gas-phase and b) particle-phase velocity profiles obtained from the present numerical analysis with the boundary-layer theory results for M_∞ = 1.5 and $Re_\infty = 10^4$ at two different regions of the flat plate.

use constant grid spacing in x direction and variable grid spacing in y direction. In the process of refinement, the number of cells in the y direction are doubled. The solutions for j max varying from 22 to 176 with i max value of 32 were obtained for refinement study in y direction, where i max is the number of cells along the flat plate from the leading edge to the trailing edge and j max is the number of cells normal to the surface. It was found that the error in various quantities such as skin-friction coefficient, wall pressure, and heat-transfer rate was less than 5% in the next to the finest grid G4 except in the regions close to the leading edge. Based on this study, we have used 32 cells along the surface and 88 cells normal to the surface of the plate.[24]

The numerical results for the dusty gas hypersonic flow over a flat plate are computed for $M_\infty = 6$, $Re_\infty = 10^6$, and mass loading

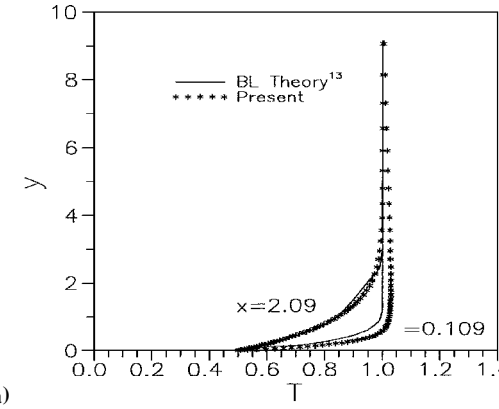

a)

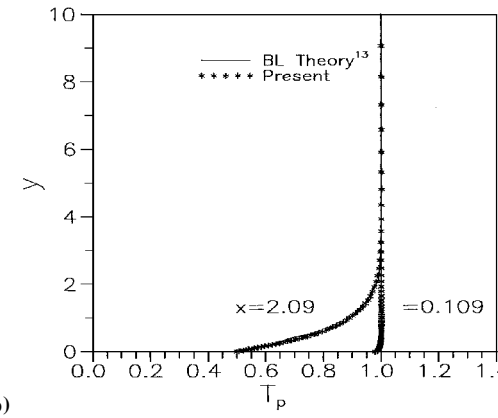

b)

Fig. 3 Comparison of a) gas-phase and b) particle-phase temperature profiles obtained from the present numerical analysis with the boundary-layer theory results for M_∞ = 1.5 and $Re_\infty = 10^4$ at two different regions of the flat plate.

ratio $\beta = 1$. The particles considered are glass spheres of uniform diameter of 10 μm with constant material density. The studies are done for isothermal wall condition. In all of the figures presented here, x is the nondimensional distance measured from the leading edge of the flat plate.

The flow profiles of tangential velocity u, normal velocity component v, and temperature T for both the phases are computed at different distances from the leading edge. From these results it is shown that the boundary-layer flow properties of the dusty gas have different characteristics in the three distinct regions shown schematically in Fig. 1. Each of these three flow regimes presents its own peculiar problems as far as the computations are concerned. Therefore, great care must be taken in order to obtain a stable and convergent finite volume solution. In the large-slip region the particles have a little deviation from their freestream uniform motion, and the differences in the flow quantities of the two phases are quite large. This is observed in the velocity and temperature profiles at $x = 0.07$ station presented in Figs. 4a and 5a. While slipping through the gas downstream, interaction between the two phases increases the gas velocity and temperature but decreases the particle velocity and temperature as well. Thus, in the transition region, the differences in the flow properties of the two phases are significantly reduced. Of course, the particles and the gas are still in nonequilibrium. In this region the velocity slip and temperature defect are moderate compared with those in the other two limiting regions. This can be observed in Figs. 4b and 5b at $x = 0.4$ station. The velocity and temperature profiles in the small-slip region are shown at $x = 2.3$ in Figs. 4c and 5c, respectively. In this region the flow profiles for the particle phase become almost identical with those for the gas phase, that is, two phases approach near equilibrium and the slip quantities are very small. Thus, the particles have enough time to alter their state appreciably and achieve quasi-equilibrium with the gas.

The three important characteristic quantities of interest in dusty-gas flow analyses are the variation of skin-friction coefficient along the wall C_f, variation of wall heat-transfer rate $\dot{q}_w$, and the

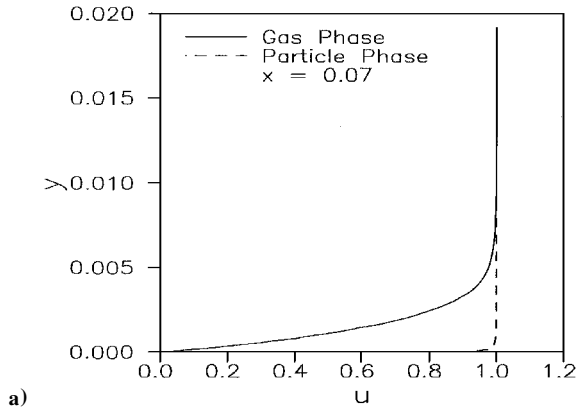

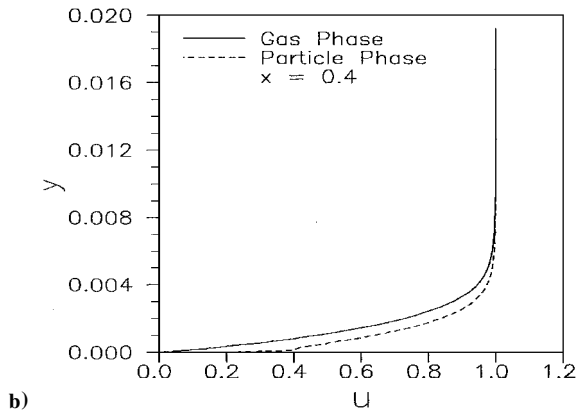

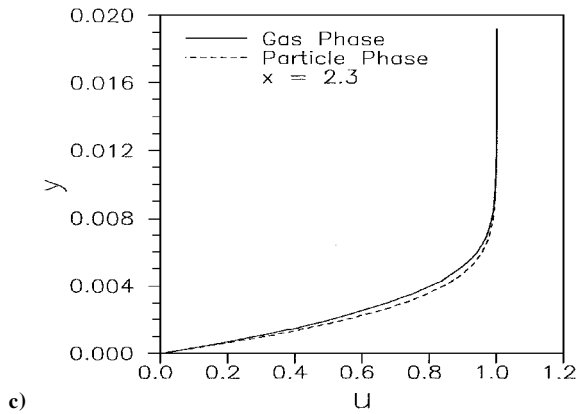

Fig. 4 Velocity profiles of the gas phase and particle phase in the a) large slip region, b) moderate slip region, and c) small slip region within the boundary layer for $M_\infty = 6$ and $Re_\infty = 10^6$.

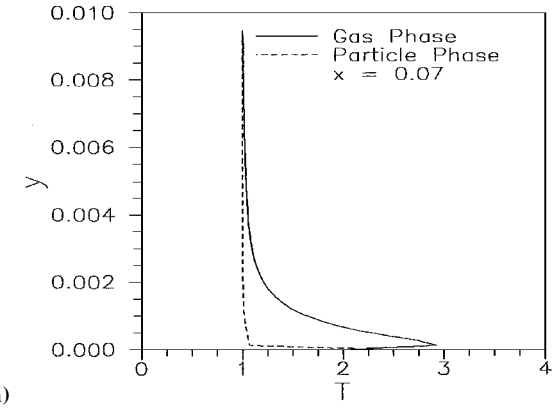

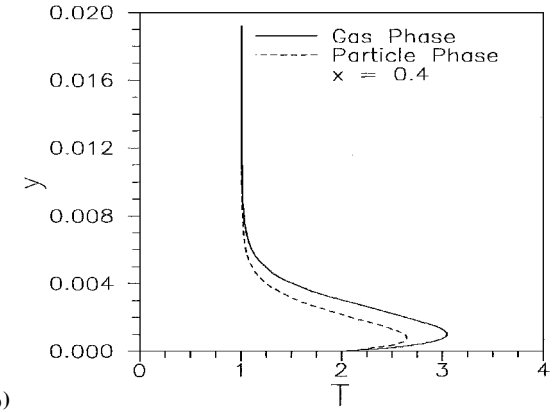

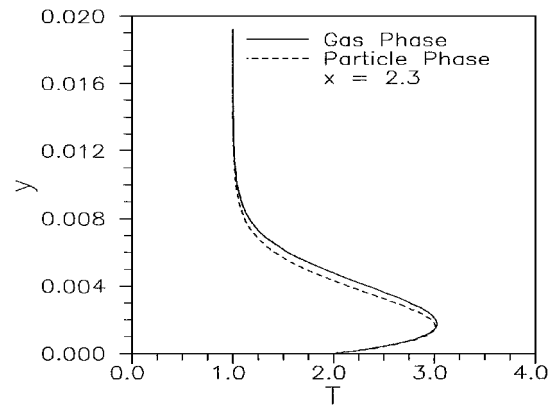

Fig. 5 Temperature profiles of the gas phase and particle phase in the a) large slip region, b) moderate slip region, and c) small slip region within the boundary layer for $M_\infty = 6$ and $Re_\infty = 10^6$.

boundary-layer thickness δ. As usual, they are determined from the flow profiles of the gas phase. It is observed that the presence of particles in the gas flow over the flat plate enhances the skin friction and heat transfer at the wall of the plate. This tendency can be seen in Figs. 6 and 7, where the skin friction and heat-transfer rate are shown as functions of nondimensional distance from the leading edge for the cases with and without particles. Physically the changes in the flow characteristics caused by the particles can be explained as follows. In presence of particles, the gas gains some kinetic and thermal energy from the particles through the interaction, and the gas velocity and temperature increase above the pure-gas case. Consequently, the gradients of the gas velocity and temperature with respect to the normal coordinate at the wall for dusty-gas flow become greater than those without particles. These changes result in an increase in the skin friction and heat transfer at the wall because they are proportional to those gradients. It is found that the curves for the skin friction and the heat-transfer rate are nearly identical except in the nonequilibrium region. In these figures it is interesting to note that along every curve for the characteristic quantities there is a inflection point that corresponds to the critical point. This means

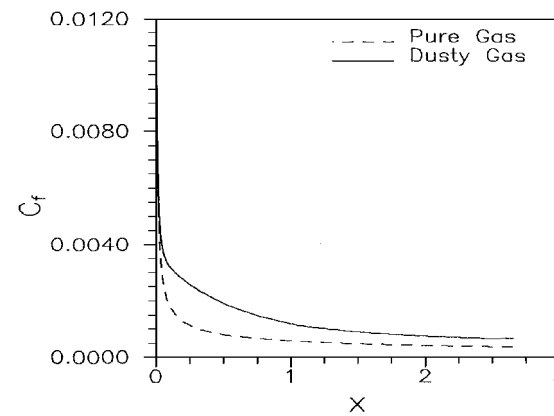

Fig. 6 Variation of the skin-friction coefficient along the flat plate in a pure- and dusty-gas hypersonic flow with $M_\infty = 6$ and $Re_\infty = 10^6$.

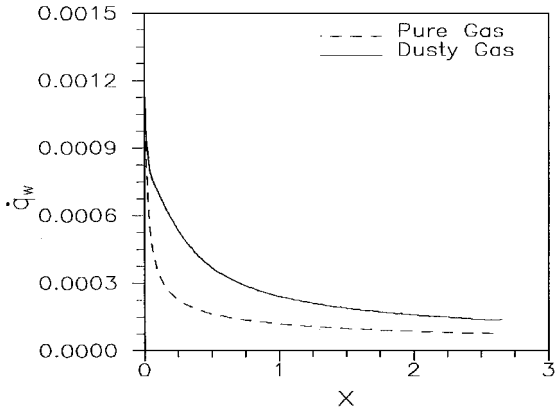

Fig. 7 Variation of the heat-transfer coefficient along the flat plate in a pure- and dusty-gas hypersonic flow with $M_\infty = 6$ and $Re_\infty = 10^6$.

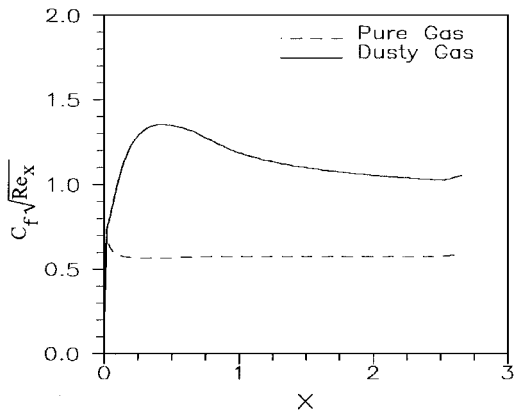

Fig. 8 Variation of the product $C_f\sqrt{Re_x}$ along the flat plate in a pure- and dusty-gas hypersonic flow with $M_\infty = 6$ and $Re_\infty = 10^6$.

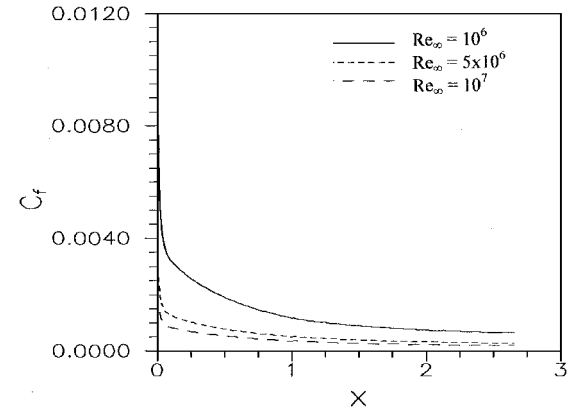

Fig. 9 Variation of the skin-friction coefficient along the flat plate in a dusty-gas hypersonic flow with different freestream Reynolds numbers and $M_\infty = 6$.

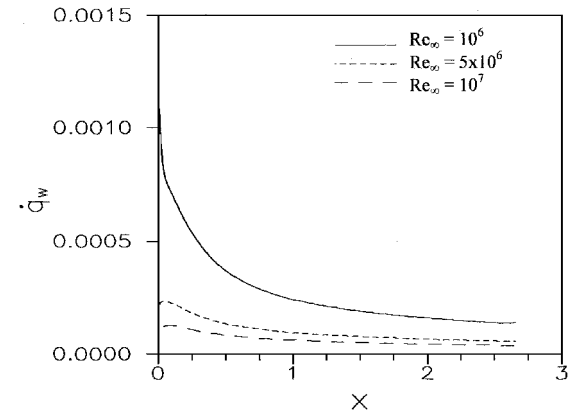

Fig. 10 Variation of the heat-transfer coefficient along the flat plate in a dusty-gas hypersonic flow with different freestream Reynolds numbers and $M_\infty = 6$.

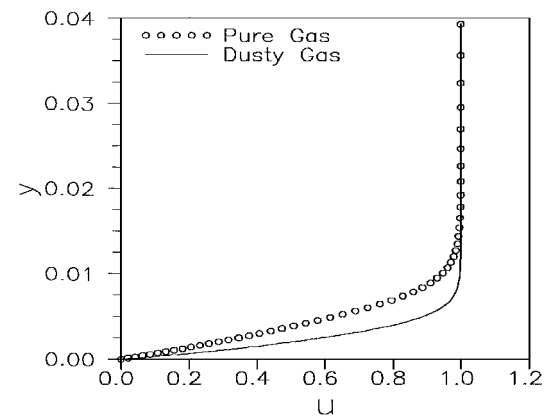

Fig. 11 Velocity profiles of the gas phase within the boundary layer at $x = 1.2$ on a flat plate for $M_\infty = 6$, $Re_\infty = 10^6$, and $T_w = 2$.

that for a boundary-layer flow for a gas particle mixture some significant changes in the flow properties occur at the critical point. In fact, as mentioned before, the two-phase system accomplishes the transition from the nonequilibrium to equilibrium flow.

The skin-friction coefficient in the form $C_f\sqrt{Re_x}$ along the flat plate for both the pure-gas and dusty-gas flow is shown in Fig. 8. When there are no particles in the gas, $C_f\sqrt{Re_x}$ should remain constant along the flat plate. Except near the leading edge, the $C_f\sqrt{Re_x}$ remains constant for the given Mach number and Reynolds number. The slight increase in the $C_f\sqrt{Re_x}$ values noticed at the leading edge is attributed to the "leading-edge error," which is bound to occur in any numerical solution. This is because in getting the numerical solution the equations are not solved for $C_f\sqrt{Re_x}$ directly, but C_f is constructed using the velocity values, and then $C_f\sqrt{Re_x}$ is calculated. It is not possible to expect infinite values of C_f at the leading edge because of the finite grid spacings. Hence, $C_f\sqrt{Re_x}$ at the leading edge has an in built error in the numerical solution and this error persists for some distance downstream. This distance can be greatly reduced if extremely fine grid spacings are chosen in x direction. The skin friction increases at all of the locations of the plate in the presence of particles compared to the pure-gas case. It is observed from the graph that the $C_f\sqrt{Re_x}$ values in the region between $x = 1.5$ and 2.5 almost double for the dusty-gas case. The variation of skin friction and heat transfer along the flat plate for $Re_\infty = 10^6$, 5×10^6, and 10^7 with $M_\infty = 6$ are plotted in Figs. 9 and 10. It is observed that the skin friction and the heat transfer decreases at all of the locations of the plate as the Reynolds number increases.

In Figs. 11 and 12 the parallel component of the velocity u and temperature T are plotted against the distance normal to the surface for both pure gas and dusty gas. The plots are presented at $x = 1.2$ station. The boundary-layer portions are zoomed and shown here. We have already seen that the skin friction and heat-transfer rate at the wall increase owing to the presence of particles. Now, owing to the interaction between the particles and the gas in the two-phase flow within the boundary layer, the tangential velocity and temperature of the gas phase increase except at the wall and at the outer edge. This is the result of choosing the same boundary conditions as chosen for the pure-gas case. Compared with the pure-gas boundary layer, the velocity and temperature profiles within the dusty-gas boundary layer have a steeper gradient at the wall and a more even gradient near the outer edge. It is observed from Fig. 13 that the boundary-layer thickness for the dusty gas is thinner than the pure-gas boundary layer because the velocity and temperatures approach their freestream values much earlier because of the enhancement of skin friction and heat transfer along the length of the plate. The dusty gas boundary-layer growth for various freestream

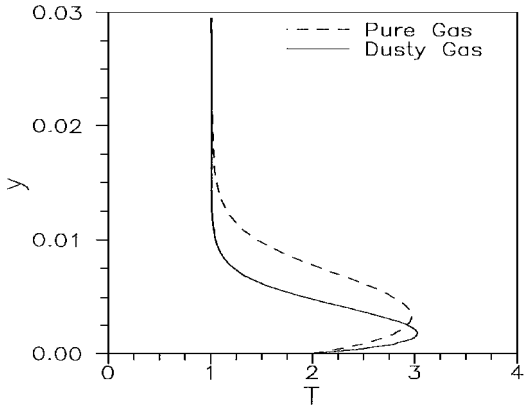

Fig. 12 Temperature profiles of the gas phase within the boundary layer at $x = 1.2$ on a flat plate for $M_\infty = 6$, $Re_\infty = 10^6$, and $T_w = 2$.

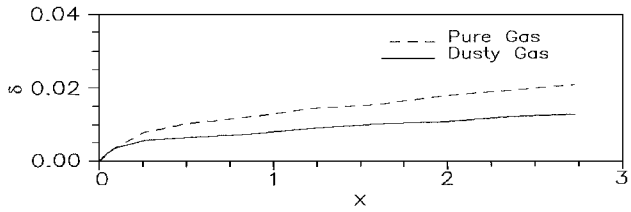

Fig. 13 Growth of the velocity boundary layer along the flat plate in a hypersonic flow with $M_\infty = 6$ and $Re_\infty = 10^6$.

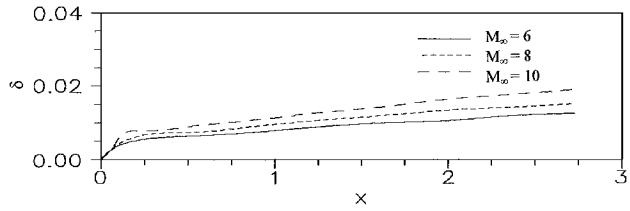

Fig. 14 Growth of the velocity boundary layer along the flat plate in a dusty-gas hypersonic flow with different freestream Mach numbers and $Re_\infty = 10^6$.

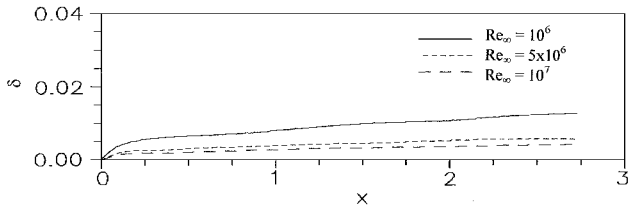

Fig. 15 Growth of the velocity boundary layer along the flat plate in a dusty-gas hypersonic flow with different freestream Reynolds numbers and $M_\infty = 6$.

Mach numbers and Reynolds numbers are presented in Figs. 14 and 15. It is observed that the boundary layer grows thicker as the Mach number increases and thinner as the Reynolds number increases. Based on the velocity profiles, boundary-layer thickness was estimated, and it is found that δ is proportional to $M_\infty^{1.3}$. The estimate also indicated that δ is inversely proportional to $\sqrt{Re_\infty}$ in conformity with the boundary-layer theory.

Conclusions

Detailed results of the analysis of the effects of the particles on the flowfield parameters in hypersonic flows are presented here. The modification in the flow properties owing to the presence of particles includes an alteration of the flow profiles, an increase in the skin friction and heat transfer at the wall, and a decrease in the boundary-layer thickness. The analysis shows that the structure of the velocity and temperature profiles are significantly altered because of the presence of particles for the freestream condition considered here. It is shown that the boundary-layer thickness is proportional to $M_\infty^{1.3}$ and $1/\sqrt{Re_\infty}$. The skin friction, wall heat transfer, and boundary-layer thickness for the dusty-gas flow increase as the freestream Mach number increases, whereas these characteristic flow quantities decrease as the Reynolds number decreases.

References

[1]Marble, F. E., "Dynamics of Dusty Gases," *Annual Review of Fluid Mechanics*, Vol. 2, 1970, pp. 397–446.

[2]Rudinger, G., *Fundamentals of Gas-Particle Flows*, Elsevier, Amsterdam, 1980, pp. 1–18.

[3]Soo, S. L., *Fluid Dynamics of Multiphase Flows*, Blaisdell, Waltham, MA, 1967.

[4]Gilbert, M., Allport, J., and Dunlap, R., "Dynamics of Two-Phase Flow in Rocket Nozzles," *ARS Journal*, Vol. 32, No. 12, 1962, pp. 1929, 1930.

[5]Probstein, R. F., and Fassio, F., "Dusty Hypersonic Flows," *AIAA Journal*, Vol. 8, No. 4, 1970, pp. 772–779.

[6]Waldman, G. D., and Reinecke, W. G., "Particle Trajectories, Heating, and Break Up in Hypersonic Shock Layers," *AIAA Journal*, Vol. 9, No. 6, 1971, pp. 1040–1048.

[7]Crowe, C. T., "Review-Numerical Models for Dilute Gas-Particle Flows," *Journal of Fluids Engineering*, Vol. 104, No. 9, 1982, pp. 297–303.

[8]Soo, S. L., "Laminar and Separated Flow of a Particulate Suspension," *Astronautica Acta*, Vol. 11, No. 6, 1965, pp. 422–431.

[9]Marble, F. E., "Dynamics of Gas Containing Small Solid Particles," *Fifth AGARD Combustion and Propulsion Colloquim*, Pergamon, Oxford, 1963, pp. 175–215.

[10]Chiu, H., "Boundary Layer Flow with Suspended Particles," Princeton Univ., Rept. 620, Princeton, NJ, Aug. 1962.

[11]Singleton, R. E., "The Compressible Gas-Solid Particle Flow over a Semi-Infinite Flat Plate," *ZAMP*, Vol. 16, No. 4, 1965, pp. 421–428.

[12]Otterman, B., "Particle Migration in Laminar Mixing of a Suspension with a Clear Fluid," *ZAMP*, Vol. 20, No. 6, 1969, pp. 730–749.

[13]Wang, B. Y., and Glass, I. I., "Compressible Laminar Boundary-Layer Flows of a Dusty Gas over a Semi-Infinite Flat Plate," *Journal of Fluid Mechanics*, Vol. 186, Jan. 1988, pp. 223–241.

[14]Hwang, C. J., and Chang, G. C., "Numerical Study of Gas-Particle Flow in a Solid Rocket Nozzle," *AIAA Journal*, Vol. 26, No. 6, 1988, pp. 682–689.

[15]Chang, H. T., Hourng, L. W., and Chien, L. C., "Application of Flux-Vector-Splitting Scheme to a Dilute Gas-Particle JPL Nozzle Flow," *International Journal for Numerical Methods in Fluids*, Vol. 22, 1996, pp. 921–935.

[16]Chamkha, A. J., "Compressible Dusty-Gas Boundary-Layer Flow over a Flat Surface," *Journal of Fluids Engineering*, Vol. 118, No. 3, 1996, pp. 179–185.

[17]Elangovan, R., "Numerical Analysis of the Relaxation of Particle and Gas Phases in Dusty Supersonic Viscous Flow," AIAA Paper 89-0686, Jan. 1989.

[18]Putnam, A., "Integrable Form of Droplet Drag Coefficient," *ARS Journal*, Vol. 31, No. 10, 1961, pp. 1467, 1468.

[19]Knudsen, J. G., and Katz, D. L., *Fluid Dynamics and Heat Transfer*, McGraw–Hill, New York, 1958, p. 5.

[20]Roe, P. L., "Approximate Riemann Solvers, Parameter Vectors and Difference Schemes," *Journal of Computational Physics*, Vol. 43, No. 2, 1981, pp. 357–372.

[21]Peyret, R., and Taylor, T. D., "Computational Methods for Fluid Flow," Springer-Verlag, New York, 1983, Chap. 3, pp. 108–112.

[22]Steger, J. L., and Warming, R. F., "Flux-Vector Splitting of the Inviscid Gas Dynamics Equations with Application to Finite Difference Methods," *Journal of Computational Physics*, Vol. 40, No. 1, 1981, pp. 263–293.

[23]Blottner, F. G., "Accurate Navier–Stokes Results for the Hypersonic Flow over a Spherical Nose Tip," *Journal of Spacecraft and Rockets*, Vol. 27, No. 2, 1990, pp. 113–122.

[24]Padmapriya, R., "Numerical Analysis of Dusty Hypersonic Viscous Gas Flow over a Flat Plate," M.S. Thesis, Dept. of Aerospace Engineering, Indian Inst. of Science, Bangalore, India, April 1998.

M. Sichel
Associate Editor